PNAS

Supporting Information for

Enhancement of the liver's neuroprotective role ameliorates traumatic brain injury pathology

Yongfeng Dai [1], Jinghua Dong [1], Yu Wu, Minzhen Zhu, Wenchao Xiong, Huanyu Li, Yulu Zhao, Bruce D Hammock [2], Xinhong Zhu [2]

[1] Y. D. and J. D. contributed equally to this work
[2] To whom correspondence may be addressed.
Email: bdhammock@ucdavis.edu (B.H.D.) or zhuxh527@126.com (X.Z.)

This PDF file includes:

Supporting Information Text

SI Material and Methods

Animals. Adult male C57BL/6J mice (8–12 weeks old) were obtained from Southern Medical University Animal Center (No: SCXK-2021-0041, Guangzhou, China). The mice were housed in ventilated cages at 24±1°C and were kept under a 12/12 h light/dark cycle (7:00 AM-7:00 PM) with *ad libitum* access to food and water. All procedures were performed in accordance with the guidelines of the Chinese Council on Animal Care. *Albumin*-CreER^{T2}; *Ephx2*$^{loxp/loxp}$ double-transgenic mice were generated as per our previous study (1). For the Cre recombinase-mediated excision of the loxp sites, 8-week-old *Albmin*-CreER^{T2}; *Ephx2*$^{loxp/loxp}$ mice were intraperitoneally injected (i.p.) with tamoxifen (100 mg/kg, Sigma-Aldrich, Cat#T5648) for 5 consecutive days, and experiments were performed 4 weeks later. Behavioral experiments were double-blindly conducted at 1:30-4:30 PM.

Virus vector construction and injection. The recombinant adeno-associated viruses (rAAV) used in this study have been previously described (1). The sequences of the shRNA targeting *Ephx2* (GenBank accession: NM_007940) were 5′-GCAGCTGATTGGAGAGTAA-3′ and 5′-GAGCC-AATCTACCTGAGAATT-3′. The negative control sequence was TTCTCCGAAC GTGTCACGT. For *Ephx2* overexpression, the mouse *Ephx2* coding sequence was amplified using the primer pair 5′ GCATGGACGAGCTGTACAAGGGAAGCGGAGCTACTA ACTT-3′ (forward) and 5′-GTTGATTATCTCGAGAATTCTCAGATCTTGGATGTCACGC-3′ (reverse) and was then cloned into the rAAV-Ef1a-eYFP vector. Mice were injected *via* the tail vein with 200 μL of saline solution containing 1×10^{11} rAAV2/8.

Controlled cortical injury. A controlled cortical injury (CCI) model was used to induce TBI in mice, as previously described (2, 3). Briefly, the mice were anesthetized with sodium pentobarbitone (80 mg/kg, i.p.) and the heads were then fixed in the stereotactic frame with a hot pack placed under the body to maintain body temperature at 37°C. An incision of 10 mm in the midline was made after cleaning the surgical area with an ethanol swab. A 4.5-mm craniotomy was made on the right side of the skull (the central point was Bregma −2.0 mm and Lateral 2.5 mm) and the skull flap was removed. The brain was tilted at an angle of 15° and placed perpendicular to the impactor (4-mm diameter tip; RWD Life Science, China). The impactor parameters for CCI were impact speed, 3.5 m/s; deformation depth, 1.30 mm; and duration, 400 ms. After CCI, the skin incision was sutured and treated with antibiotic ointment to prevent infection. Then, the mice were placed on a heat pad to maintain core body temperature until they had recovered from anesthesia. For the sham group, a craniotomy was also performed and the dura was exposed, but no impact was made.

Closed head injury. A closed head injury (CHI) model of diffuse TBI in mice was operated as previously described (4). Briefly, the mice were anesthetized and the head was stabilized in the stereotactic frame. A 4-mm diameter tip was used to deliver a single controlled impact (the central point was Bregma −2.0 mm and Lateral 2.5 mm) with controlled velocity (5.0 m/s), dwell time (100 ms) and impact depth (1.0 mm). The study excluded mice with depressed skull fractures or visible hemorrhages. The same surgical procedure was performed on sham-injured mice, but had no impact.

Open field test. The open field test was conducted as previously described (5). The device consisted of an open rectangular box with detectors on all sides (40×40×30 cm, Accuscan Instruments, Columbus, OH, USA). Mice were first acclimated to the experimental room for 1 h. During the experiment, the animals were placed in the center of the box and allowed to freely explore for 30 min. The total distance traveled was calculated using Versmax analysis software. The open field test was performed 2 days after CCI induction. All experiments and data analyses were performed in a blinded manner.

Rotarod test. The rotarod test was performed as previously described (6). Mice were first trained at a constant speed for 3 days. During the test phase, the mice were placed on an accelerating

rotarod, with the speed increasing from 4 to 40 rpm over 5 min. The time it took for the mice to fall off the rod was recorded and each mouse was trained for 5 trials (5 min running and 5 min resting for each trial). Finally, the average of 5 running times was determined. The rotarod test was performed at 1day pre-CCI and 1, 3 days post- CCI. All experiments and data analyses were performed in a blinded manner.

Y-maze test. The Y-maze consisted of three identical long arms (30×10×20 cm) spaced at 120° angles. The mice were first allowed to adapt to the experimental environment for 1 h before the experiment. The animals were then placed in the central area and allowed to freely explore the maze for 5 min while their movements were recorded by a camera placed above the maze. Mice were considered to have made a choice when they had fully entered a long arm; three different consecutive choices were considered an alternation. The alternation percentage was calculated using the following formula: total alternations/ (total choices−2) × 100. The experiment was performed at 4 days post-CCI. All experiments and data analyses were performed in a blinded manner.

Measurement of brain edema. As previously described (7), cerebral edema was detected using the wet–dry weight method. After the mice had been euthanized, their brains were quickly removed and placed in a pre-cooled saline solution to remove excess blood and pollutants. The surface of the brain was drained and both the injured and contralateral cortex were weighed. The cortex was then dehydrated in a drying oven at 100–110°C for more than 24 h and reweighed. The percentage of brain tissue water content was calculated as follows: (wet weight−dry weight)/wet weight × 100.

Blood-brain barrier (BBB) permeability assay. BBB permeability was determined using Evans blue extravasation (8). Briefly, mice were injected with Evans blue (2%, 4 mL /kg, Macklin, Cat#E6135) in 0.9% saline via the tail vein 4 days after CCI. One hour later, the mice were anesthetized and perfused with 0.1 M PBS, and the brains were removed and photographed. Ipsilateral brains were immediately weighed and homogenized in 1 mL of 60% trichloroacetic acid solution (Macklin, Cat#T834457). The absorbance of the supernatant was measured at OD620 nm. In accordance with a standard curve, the EB concentrations were calculated and expressed as μg/g brain tissue.

Tissue preparation for histology and immunostaining. Mice were deeply anesthetized with sodium pentobarbitone (160 mg/kg, i.p.) and perfused with pre-cooled saline solution to drain the blood, and then with 4% paraformaldehyde (PFA). The brains of the mice were removed intact from the skull, post-fixed by immersion in 4% PFA, rinsed, and then dehydrated in 30% sucrose solution. Coronal sections (40-μm thick) were obtained in a freezing microtome (Leica, CM1950) starting at Bregma −0.46 mm. Seven sections, 480-μm apart, were selected for NeuroTrace 500/525 Green Fluorescent Nissl staining and used to calculate the lesion volume, while the remaining coronal sections were used for immunofluorescence staining.

Assessment of lesion volume. Coronal sections were subjected to Nissl staining. In brief, sections were washed with 0.1 M PBS containing 0.3% Triton X-100 and then incubated for 20 min with NeuroTrace 500/525 Green Fluorescent Nissl (1:300, Invitrogen, Cat#N21480), followed by washing. The sections were mounted in Vectashield Antifade Mounting Medium with DAPI (Vector Laboratories, Cat#H-1200), covered with glass coverslips, and imaged at ×4 magnification objective using an Olympus VS200 microscope equipped with Olyxia analysis software. To quantify the lesion area of sections, the brain atlas was mapped onto each section to outline the whole section, as previously described (9). ImageJ analysis software (US National Institutes of Health) was used to calculate the lesion area. Lesion volume (V, mm^3) was calculated using the following formula: $V = (S1+S2+...+S7) \times d$, where S is the lesion area (in mm^2) and d is the distance between sections (0.48 mm).

Immunofluorescence staining. Immunofluorescence staining was performed using the 40-μm-thick coronal sections. For each mouse, three slices close to the center of the CCI impact site

(between Bregma −1.5 mm and −2.5 mm) were chosen. Brain sections were rinsed three times with 0.1 M PBS, blocked with 10% BSA containing 0.3% Triton X-100 for 2 h, and rinsed. The sections were then incubated with primary antibodies (rabbit anti-Iba-1, 1: 500, Wako, Cat#019-19741; and mouse anti-GFAP, 1: 500, Cell Signaling Technology, Cat#3670S) at 4°C for more than 16 h, rinsed with 0.1 M PBS, incubated with secondary antibody for 2 h at room temperature in the dark (Alexa Fluor 488-conjugated donkey anti-rabbit IgG, 1: 500, Invitrogen, Cat# A21206; and Alexa Fluor 488-conjugated donkey anti-mouse IgG, 1: 500, Invitrogen, Cat# A21202), washed, mounted in Vectashield Antifade Mounting Medium containing DAPI, and cover slipped. Immunofluorescence images of the perilesional cortex and the hippocampal dentate gyrus were captured using a Nikon A1R confocal microscope (Nikon Instrument Inc.) at ×40 or x20 magnification objective. Cell covered area, number, and mean intensity were calculated using ImageJ analysis software while the cell volume was calculated by 3-D rendering and analysis with Imaris 9.6 (Bitplane, USA), as previously described (10).

TUNEL assay. Apoptosis was assessed using a (TUNEL) kit (Yeasen, Cat#40308ES60) following the manufactures' introduction. Briefly, 40 μm brain sections were incubated in TUNEL reaction mixture for 1 h in the dark (37°C). Nuclei were visualized using DAPI. TUNEL+ cells and DAPI+ cells were captured using a Nikon A1R confocal microscope.

EETs measurements. UPLC–MS/MS analysis was used to measure plasma 14,15-EET levels as per our previous report (1). Briefly, blood was drawn into EDTA-coated tubes and centrifuged at 3,500 rpm for 15 min. Next, sEH inhibitor trans-4-{4-[3-(4-trifluoromethoxy-phenyl)-ureido]-cyclohexyloxy}-benzoic acid (*t*-TUCB,800 nM, Tocris Bioscience, Cat# 6757) was added to the plasma supernatant. For brain tissue, the cortex was immediately weighed and homogenized in 0.1 M PBS containing another sEH inhibitor 1-trifluoromethoxyphenyl- 3-(1-propionylpiperidin-4-yl) urea (TPPU, 10 μM, MCE, Cat#HY-101294). Plasma or cortex suspension (200 μL) were then mixed with methanol (200 μL) containing internal standard (11,12-EET-d_{11}, 20 ng/mL, Cayman, Cat#10006413) and the mixture was vortexed at 4,500 rpm for 10 min at 4°C and centrifuged at 6,000 rpm (4°C) for 1 min. The samples were placed at −80°C for protein precipitation for 2 h, centrifuged at 14,000 rpm for 10 min at 4°C, and the supernatant was collected by filtration for UPLC–MS/MS analysis. Data were collected using Tracefinder 4.1 software (Thermo Fisher Scientific).

Measurement of sEH activity. sEH protein hydrolyzes 14,15-EET to 14,15-DHET, and the activity of sEH is determined according to the content of the metabolite 14.15-DHET. Deeply anesthetized mice were perfused with saline solution, and then the peripheral organs (liver, kidney, heart, spleen, lung) and the cortex were immediately collected. The tissues were homogenized in 0.1 M PBS (10 μL/mg) and then centrifuged at 9,000 × *g* for 10 min at 4°C. The supernatant was collected and the protein content was measured using the Pierce BCA Protein Detection Kit (Thermo Fisher Scientific, Cat# 23225). The expression of sEH is known to vary among different organs (11). Quantified supernatants of liver, kidney, heart, spleen, lung, and cortex were diluted with 0.1 M PBS at a ratio of 1:450, 1:300, 1:100, 1:20, 1:2 and 1:20, respectively. Then, 20 μL of diluted protein solution, 160 μL of PBS, and 10 μL of 14,15-EET (10μg/mL) were mixed and incubated at 37°C for 1 h. The reaction was terminated by adding 10 μL of *t*-TUCB (800 nM). Subsequently, the levels of metabolite 14,15-DHET were measured following the EETs measurements protocol.

Assessment of 14,15-EET crossing the BBB. Deuterium-labelled 14,15-EET (14,15-EET-d_{11}, Cayman, Cat# 10006410) was used as a tracer to determine whether 14,15-EET could cross the BBB. Carotid cannulation is performed as previously described (12). Briefly, adult male C57BL/6J mice were pre- treated with TPPU (10 mg/kg, i.p.) for 3 h and 0.5 h before the surgery. The right common carotid artery (CCA), external carotid artery (ECA), and internal carotid artery (ICA) were isolated using a stereomicroscope (SMZ745T, Nikon). Then, the external jugular vein was ligated, the common carotid artery was cut, and a 0.2 mm catheter (RWD Life Science) was inserted into the CCA. 14,15-EET-d_{11} (500ng in 100 μL ACSF) or vehicle (ACSF) was injected at a rate of 4 μL/s through the catheter. 1 min after injection, blood was drawn into EDTA-coated tubes to

collect the plasma. After the mice were perfused with 0.1 M PBS, the cortex was immediately weighed and homogenized in 0.1 M PBS containing TPPU (10 μM). Plasma and brain levels of 14,15-EET-d_{11} and 14,15-DHET-d_{11} were measured following the EETs measurements protocol.

Drugs and route of administration.14,15-EET and 14,15-EEZE were obtained from Cayman Chemical (14,15-EET, Cat# 50651; 14,15-DHET, Cat# 10006998). Drug solution (1 μg in 2.5 μL ACSF) was directly dripped onto the brain surface through sutured gaps at 30 minutes after surgery (Sham or CCI). Approximately 30 min before the behavioral experiment, the mice were briefly anesthetized with isoflurane and the compound was administered once a day.

Western blotting. Following perfusion with 0.1 M PBS, the liver and injured cortex of mice were collected and homogenized in RIPA lysis buffer (Beyotime, Cat#P0013B) containing 1% PMSF. After centrifugation at 14,400 rpm for 20 min at 4°C, the supernatant was collected and the protein concentration was determined. Equal amounts of protein were separated using 10%-12% SDS–PAGE and then transferred to a PVDF membrane (Merck, Cat#IPVH00010). The membranes were then incubated with primary antibodies (rabbit anti-sEH, 1: 5,000, Cayman, Cat#13560; mouse anti-GAPDH, 1: 10,000, Proteintech, Cat#60004-1-Ig; rabbit anti-MMP-9, 1: 1,000, Cayman, Cat#283575; and rabbit anti-BDNF, 1: 1,000, Cayman, Cat#108319) and then with secondary antibodies (horseradish peroxidase-conjugated AffiniPure goat anti-rabbit IgG, 1: 10,000, ZSGB-Bio, Cat# ZB2301; and goat anti-mouse IgG, 1: 10,000, ZSGB-Bio, Cat#ZB2305). GAPDH was used for normalization. All data were analyzed using ImageJ.

Quantitative Real-time PCR (qRT-PCR). Total mRNA was extracted from the liver and the injured cortex using RNAiso Plus (TaKaRa, Cat#9109) following the manufacturer's instructions and quantified using a NanoDrop 2000 (Thermo Fisher Scientific). The extracted mRNA was reverse transcribed into cDNA in a T100 Thermal Cycler (BIO-RAD) using the PrimeScript RT Reagent Kit with gDNA Eraser (TaKaRa, Cat#RR047A). qRT-PCR was performed using TB Green Premix Ex Taq (TaKaRa, Cat#RR420A) in a 7500 Real-Time PCR System (Thermo Fisher Scientific). Relative mRNA expression levels were calculated using the ΔΔCt method as previously described (13). The *Rp18s* mRNA gene was used for normalization. The sequences of all the primers used for qRT-PCR are listed in **Table S1.**

Statistical analyses. Data were analyzed using GraphPad Prism 9.0 (GraphPad Software). Data are presented as means ± SEM. Two-tailed unpaired student's *t*-tests or multiple *t*-tests were used to compare differences between two groups. One-way ANOVA with Dunnett's post-hoc test (when equal variance was assumed) or Brown-Forsythe and Welch ANOVA followed by Dunnett's T3 post-hoc test (when no equal variance was assumed) was used to compare differences between three or more groups. Two-way ANOVA followed by Bonferroni's multiple-comparisons test was used when comparing differences between two groups with two factors and repeated measures. Pearson's correlation was used for correlation analysis. *p*-values < 0.05 were considered significant.

SI Figures and Table

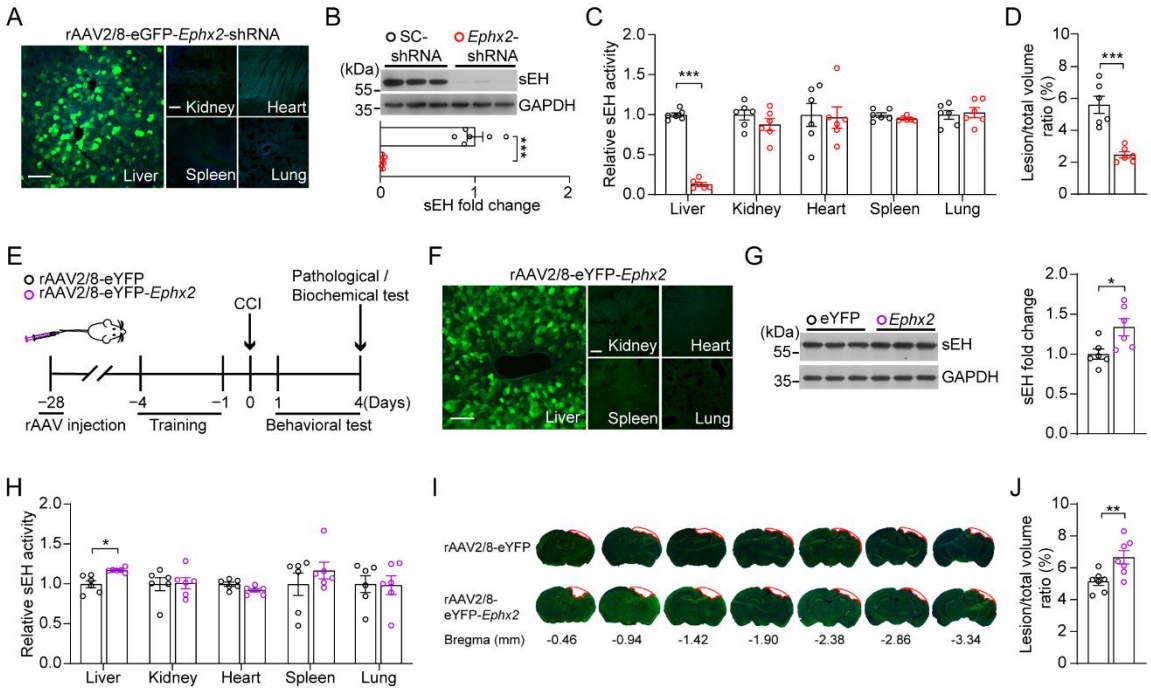

Fig. S1. The effect of hepatic sEH manipulation on peripheral organs. (*A*) rAAV2/8-eGFP-*Ephx2*-shRNA was specifically expressed in the liver 14 days after a tail-vein injection. Scale bar: 100 μm. (*B*) Western blotting and quantification of hepatic sEH in rAAV2/8-eGFP-SC and rAAV2/8-eGFP-*Ephx2*-shRNA mice (n = 6). (*C*) Relative sEH activity in the liver, kidney, heart, spleen, and lung following knocking-down hepatic sEH (n = 6). (*D*) Quantitative analysis of lesion volume percentage (n = 6). (*E*) Schematic diagram of the experimental design for overexpression of sEH in the liver. (*F*) eYFP was specifically expressed in the liver 28 days after rAAV2/8-eYFP-*Ephx2*-injection. Scale bar: 100 μm. (*G*) Western blotting and quantification of hepatic sEH in rAAV2/8-eYFP and rAAV2/8-eYFP-*Ephx2* mice (n = 6). (*H*) Relative sEH activity in the liver, kidney, heart, spleen, and lung in rAAV2/8-eYFP and rAAV2/8-eYFP-*Ephx2* mice (n = 6). (*I*) Representative images of Nissl staining for brain injury in rAAV2/8-eYFP mice and rAAV2/8-eYFP-*Ephx2* mice. The red outline represents the loss area of injured brain. (*J*) Quantitative analysis of lesion volume percentage (n = 7) following hepatic sEH overexpression. Statistical significance was determined using two-tailed unpaired student's *t*-test for *B, D, G, J*; or multiple *t*-tests for *C, H*. Data are presented as the means ± SEM. Asterisks indicate significant differences (*p < 0.05, **p < 0.05, ***p < 0.001).

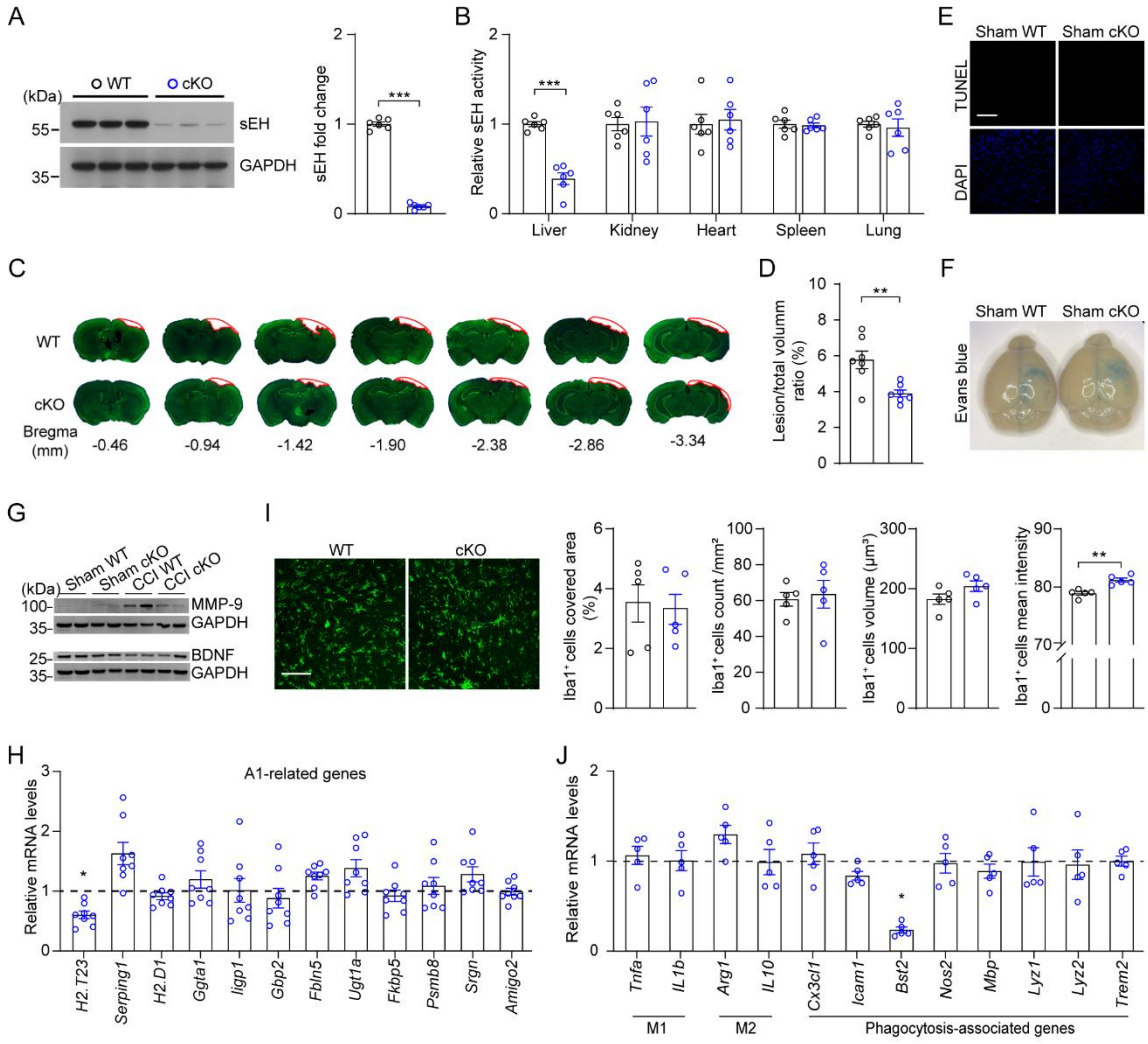

Fig. S2. Effects of hepatic *Ephx2* deletion on peripheral organs and injured cortex following CCI. (*A*) Western blotting and quantification of hepatic sEH in WT and cKO mice (n = 6). (*B*) Relative sEH activity in the liver, kidney, heart, spleen, and lung in WT and cKO mice (n = 6). (*C*) Representative images of Nissl staining of brain injury in WT and cKO mice. The red outline represents the loss area of injured brain. (*D*) Quantitative analysis of lesion volume percentage (n = 7). (*E*) No TUNEL+ cells were found in Sham-WT and Sham-cKO mice. (*F*) Representative images of Evans blue extravasation in Sham-WT and Sham-cKO mice. (*G*) Representative western blot images of anti-MMP-9 and anti-BDNF in WT and cKO mice 4 days after surgery (Sham or CCI). (*H*) Relative mRNA levels of genes associated A1 phenotype astrocytes in the injured cortex (dashed line indicated the mean levels of each corresponding gene in WT controls, n = 8). (*I*) Representative images of Iba-1+ microglia in the injured cortex; the proportion of covered area, number, volume, and mean intensity of Iba-1+ microglia were quantitatively analyzed (n = 5). Scale bar: 100 μm. (*J*) Relative mRNA levels of genes associated with M1, M2, and phagocytic function of microglia in the injured cortex (dashed line indicated the mean levels of each corresponding gene in WT controls; n = 5). Statistical significance was determined using two-tailed unpaired student's *t*-test for *A, D, I;* or multiple *t*-tests for *B, H, J*. Data are presented as the means ± SEM. Asterisks indicate significant differences (*p < 0.05, **p < 0.01, ***p < 0.001).

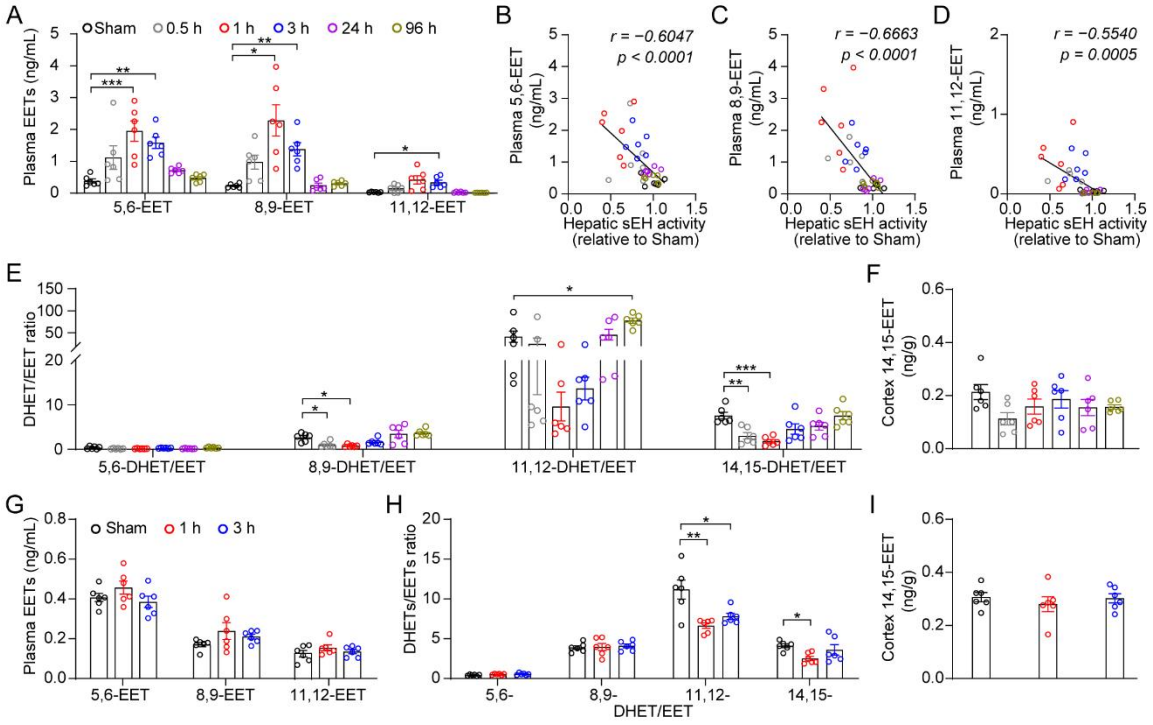

Fig. S3. Plasma and brain EETs levels in adult C57BL/6J mice following TBI. (*A*) Plasma levels of the other three isoforms of EETs, including 5,6-, 8,9- and 11,12-EET following CCI (*n* = 6 per time point). (*B*–*D*) Correlations between hepatic sEH activity and plasma EETs. (*E*) Plasma DHETs/EETs ratio following CCI (*n* = 6 per time point). (*F*) 14,15-EET levels in the injured cortex following CCI (*n* = 6 per time point). (*G*) Plasma levels of EETs following CHI (*n* = 6 per time point). (*H*) Plasma DHETs/EETs ratio following CHI (*n* = 6 per time point). (*I*) The cortex levels of 14,15-EET following CHI (*n* = 6 per time point). Statistical significance was determined using one-way ANOVA with the Dunnett's post-hoc test, or Brown-Forsythe and Welch ANOVA followed by the Dunnett's T3 post-hoc test for *A, E, F, G, H, I*; or the Pearson's correlation analysis for *B, C, D*. Data are presented as the means ± SEM. Asterisks indicate significant differences (**p* < 0.05, ***p* < 0.01, ****p* < 0.001).

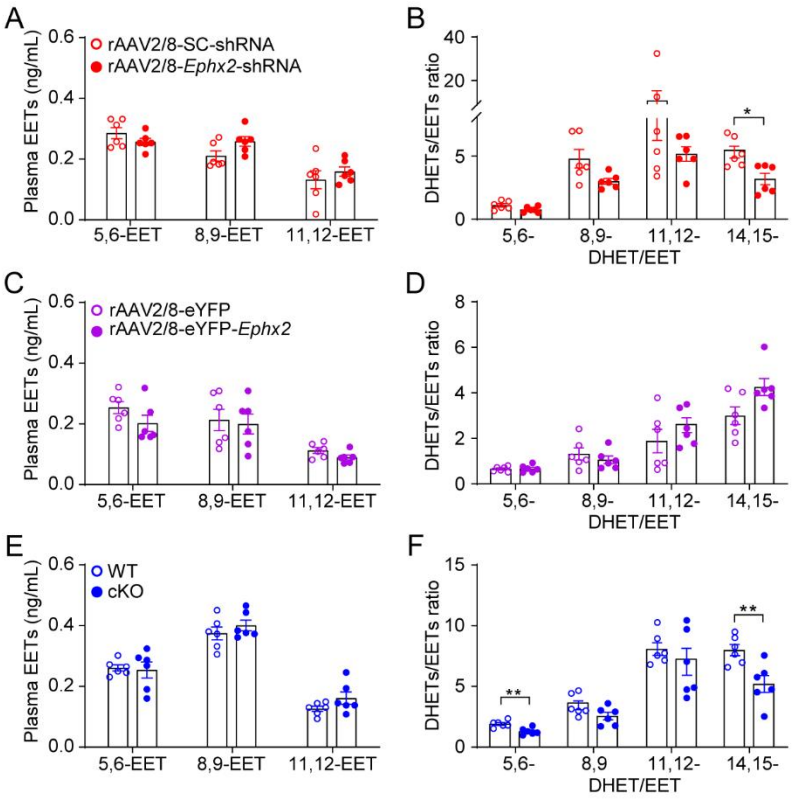

Fig. S4. Effects of hepatic sEH manipulation on plasma levels of EETs and DHETs. (*A–F*) Plasma levels of 5,6-, 8,9- and 11,12-EET (*A, C, E*), and DHETs/EETs ratio (*B, D, F*) in rAAV2/8-eGFP-*Ephx2*-shRNA mice, rAAV2/8-eYFP-*Ephx2* mice, cKO mice and their respective littermate controls ($n = 6$). Statistical significance was determined by multiple *t*-tests. Data are presented as the means ± SEM. Asterisks indicate significant differences (*$p < 0.05$, **$p < 0.01$).

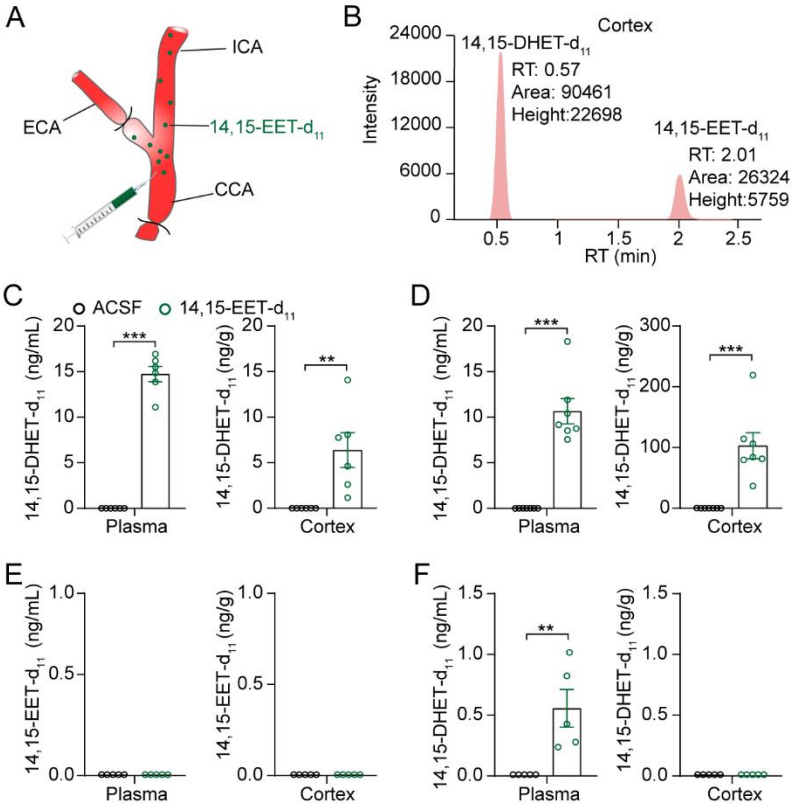

Fig. S5. 14,15-EET can rapidly cross the blood-brain barrier. (*A*) Schematic illustration of injecting 14,15-EET-d_{11} into the carotid artery. CCA: Common Carotid Artery, ECA: External Carotid Artery, ICA: Internal Carotid Artery. (see Methods for details) (*B*) Representative mass spectrogram of 14,15-EET-d_{11} and 14,15-DHET-d_{11} in the cortex detected by UPLC–MS/MS analysis. RT: Retention Time (*C*) The levels of 14,15-DHET-d_{11} in plasma and cortex of C57BL/6J mice 1 min after injection of 14,15-EET-d_{11} or ACSF (n = 6). (*D*) 14,15-DHET-d_{11} levels in the plasma and injured cortex of CCI mice 1 minute after injection of 14,15-EET-d_{11} or ACSF (n = 7). (*E, F*) The levels of 14,15-EET-d_{11} (*E*) and 14,15-DHET-d_{11} (*F*) in the plasma and cortex of C57BL/6J mice 30 min after 14,15-EET-d_{11} injected (n = 5). Statistical significance was determined using two-tailed unpaired student's *t*-test. Data are presented as the means ± SEM. Asterisks indicate significant differences (**p < 0.01, ***p < 0.001).

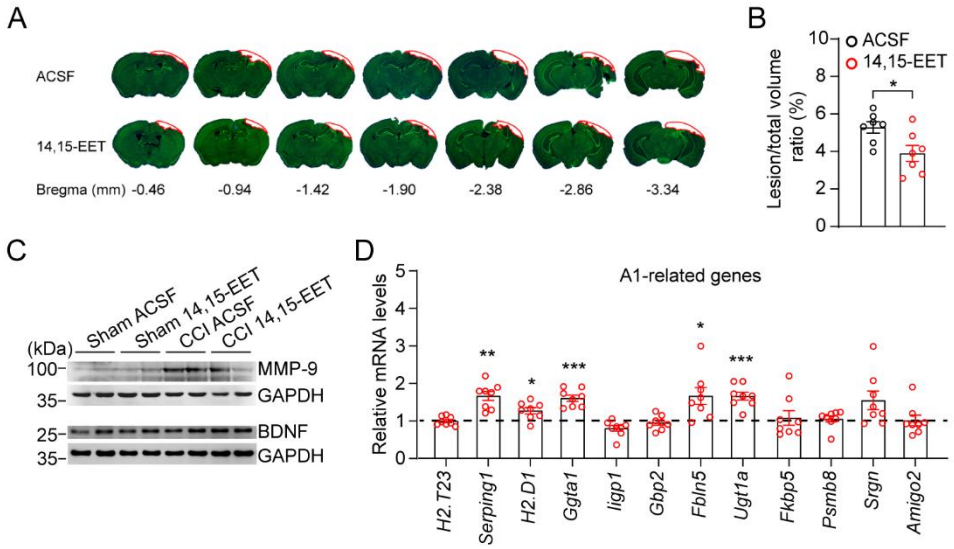

Fig. S6. The effects of 14,15-EET application on protein levels of MMP-9 and expressions of genes related to A1 astrocytes. (*A*) Representative images of brain Nissl staining for the ACSF- and 14,15-EET-treated mice following CCI. The red outline represents the loss area of injured brain. (*B*) Quantitative analysis of lesion volume percentage (n = 7). (*C*) Representative western blot images of anti-MMP-9 and anti-BDNF in mice with or without 14,15-EET treatment 4 days after surgery (Sham or CCI). (*D*) Relative mRNA levels of genes associated with A1 phenotype astrocytes in the injured cortex (dashed line indicated the mean levels of each corresponding gene in ACSF-treated controls, n = 8). Statistical significance was determined using two-tailed unpaired student's t-test for *B*, or multiple t-tests for *D*. Data are presented as the means ± SEM. Asterisks indicate significant differences (*p < 0.05, **p < 0.01, ***p < 0.001).

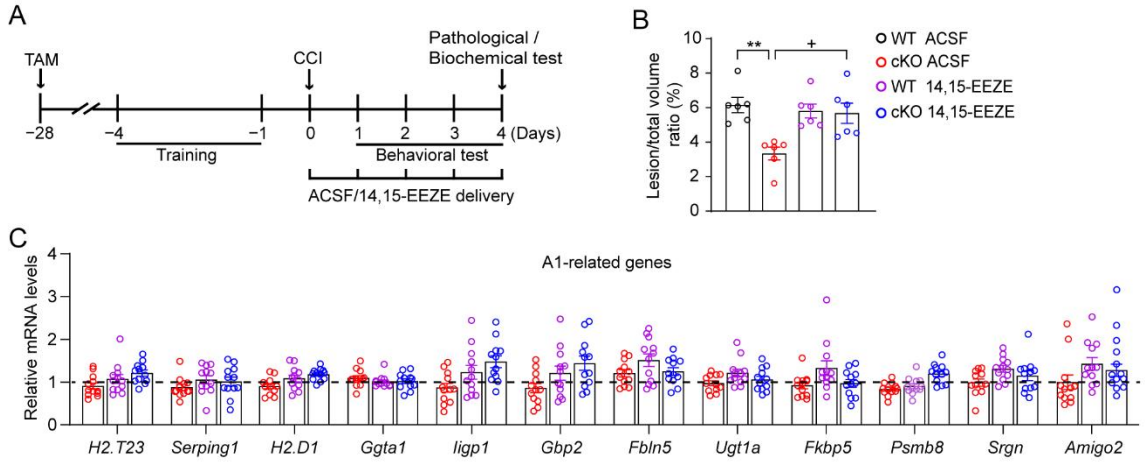

Fig. S7. The effect of 14,15-EEZE application on the expressions of genes related to A1 astrocytes in cKO and WT mice. (*A*) Schematic diagram of the experimental design.TAM: tamoxifen. (*B*) Quantitative analysis of lesion volume percentage (n = 6). (*C*) Relative mRNA levels of genes associated with A1 phenotype astrocytes in the injured cortex (dashed line indicated the mean levels of each corresponding gene in WT controls treated with ACSF; n = 12). Statistical significance was determined using two-way ANOVA followed by the Bonferroni's post-hoc test. Data are presented as the means ± SEM. Asterisks or plus signs indicate significant differences (**p < 0.01 *vs*. ACSF-treated WT mice; ^{+}p < 0.05 *vs*. ACSF-treated cKO mice).

Table S1. The sequences of the primers used for quantitative real-time PCR

Gene	Forward primer (5′–3′)	Reverse primer (5′–3′)
Tgf-β1	CTCCCGTGGCTTCTAGTGC	GCCTTAGTTTGGACAGGATCTG
Igf-1	CTGGACCAGAGACCCTTTGC	GGACGGGGACTTCTGAGTCTT
Bdnf	TCATACTTCGGTTGCATGAAGG	AGACCTCTCGAACCTGCCC
Lif	ATTGTGCCCTTACTGCTGCTG	GCCAGTTGATTCTTGATCTGGT
H2.T23	GGACCGCGAATGACATAGC	GCACCTCAGGGTGACTTCAT
Serping1	ACAGCCCCCTCTGAATTCTT	GGATGCTCTCCAAGTTGCTC
H2.D1	TCCGAGATTGTAAAGCGTGAAGA	ACAGGGCAGTGCAGGGATAG
Ggta1	GTGAACAGCATGAGGGGTTT	GTTTTGTTGCCTCTGGGTGT
Iigp1	GGGGCAATAGCTCATTGGTA	ACCTCGAAGACATCCCCTTT
Gbp2	GGGGTCACTGTCTGACCACT	GGGAAACCTGGGATGAGATT
Fbln5	CTTCAGATGCAAGCAACAA	AGGCAGTGTCAGAGGCCTTA
Ugt1a	CCTATGGGTCACTTGCCACT	AAAACCATGTTGGGCATGAT
Fkbp5	TATGCTTATGGCTCGGCTGG	CAGCCTTCCAGGTGGACTTT
Psmb8	CAGTCCTGAAGAGGCCTACG	CACTTTCACCCAACCGTCTT
Srgn	GCAAGGTTATCCTGCTCGGA	TGGGAGGGCCGATGTTATTG
Amigo2	GAGGCGACCATAATGTCGTT	GCATCCAACAGTCCGATTCT
Clcf1	CTTCAATCCTCCTCGACTGG	TACGTCGGAGTTCAGCTGTG
Tgm1	CTGTTGGTCCCGTCCCAAA	GGACCTTCCATTGTGCCTGG
Ptx3	AACAAGCTCTGTTGCCCATT	TCCCAAATGGAACATTGGAT
S100a10	CCTCTGGCTGTGGACAAAAT	CTGCTCACAAGAAGCAGTGG
Sphk1	GATGCATGAGGTGGTGAATG	TGCTCGTACCCAGCATAGTG
Cd109	CACAGTCGGGAGCCCTAAAG	GCAGCGATTTCGATGTCCAC
Ptgs2	GCTGTACAAGCAGTGGCAAA	CCCCAAAGATAGCATCTGGA
Emp1	GAGACACTGGCCAGAAAAGC	TAAAAGGCAAGGGAATGCAC
Slc10a6	GCTTCGGTGGTATGATGCTT	CCACAGGCTTTTCTGGTGAT
Tm4sf1	GCCCAAGCATATTGTGGAGT	AGGGTAGGATGTGGCACAAG
B3gnt5	CGTGGGGCAATGAGAACTAT	CCCAGCTGAACTGAAGAAGG
Cd14	GGACTGATCTCAGCCCTCTG	GCTTCAGCCCAGTGAAAGAC
Tnfα	CAGGCGGTGCCTATGTCTC	CGATCACCCCGAAGTTCAGTAG
IL1β	GAAATGCCACCTTTTGACAGTG	TGGATGCTCTCATCAGGACAG
Arg1	CAGAAGAATGGAAGAGTCAG	CAGATATGCAGGGAGTCACC
IL10	GCTCTTACTGACTGGCATGAG	CGCAGCTCTAGGAGCATGTG
Cx3cl1	ACGAAATGCGAAATCATGTGC	CTGTGTCGTCTCCAGGACAA
Icam1	AGATCACATTCACGGTGCTGGCTA	AGCTTTGGGATGGTAGCTGGAAGA
Bst2	TGTTCGGGGTTACCTTAGTCA	GCAGGAGTTTGCCTGTGTCT
Nos2	GTGTTCCACCAGGAGATGTTG	CTCCTGCCCACTGAGTTCGTC
Mbp	GGCCAGTAAGGATGGAGAGAT	CCTCTGAGGCCGTCTGAGA
Lyz1	CGTTGTGAGTTGGCCAGAA	GCTAAACACACCCAGTCAGC
Lyz2	TGAACGTTGTGAGTTTGCCA	TGAGCTAAACACACCCAGTCG
Trem2	AGGGCCCATGCCAGCGTGTGGT	CCAGAGATCTCCAGCATC
Rp18s	AGTTCCAGCACATTTTGCGAG	TCATCCTCCGTGAGTTCTCCA

SI References

1. Qin XH*, et al.* (2019) Liver Soluble Epoxide Hydrolase Regulates Behavioral and Cellular Effects of Chronic Stress. *Cell Rep* 29(10):3223-3234 e3226.
2. Smith DH*, et al.* (1995) A model of parasagittal controlled cortical impact in the mouse: cognitive and histopathologic effects. *J Neurotrauma* 12(2):169-178.
3. Wu Y*, et al.* (2021) Mild traumatic brain injury induces microvascular injury and accelerates Alzheimer-like pathogenesis in mice. *Acta neuropathologica communications* 9(1):74.
4. Bachstetter AD*, et al.* (2015) Attenuation of traumatic brain injury-induced cognitive impairment in mice by targeting increased cytokine levels with a small molecule experimental therapeutic. *Journal of neuroinflammation* 12:69.
5. Xiong W*, et al.* (2019) Astrocytic Epoxyeicosatrienoic Acid Signaling in the Medial Prefrontal Cortex Modulates Depressive-like Behaviors. *J Neurosci* 39(23):4606-4623.
6. Kim H*, et al.* (2020) Activation of the Akt1-CREB pathway promotes RNF146 expression to inhibit PARP1-mediated neuronal death. *Sci Signal* 13(663).
7. Zhao X*, et al.* (2017) Neutrophil polarization by IL-27 as a therapeutic target for intracerebral hemorrhage. *Nat Commun* 8(1):602.
8. Banerjee A*, et al.* (2011) Bacterial Pili exploit integrin machinery to promote immune activation and efficient blood-brain barrier penetration. *Nature communications* 2:462.
9. Liu S*, et al.* (2019) Induction of Neuronal PI3Kgamma Contributes to Endoplasmic Reticulum Stress and Long-Term Functional Impairment in a Murine Model of Traumatic Brain Injury. *Neurotherapeutics* 16(4):1320-1334.
10. Chen W*, et al.* (2020) 14,15-Epoxyeicosatrienoic Acid Alleviates Pathology in a Mouse Model of Alzheimer's Disease. *J Neurosci* 40(42):8188-8203.
11. Harris TR & Hammock BD (2013) Soluble epoxide hydrolase: gene structure, expression and deletion. *Gene* 526(2):61-74.
12. Colombani AL*, et al.* (2009) Enhanced hypothalamic glucose sensing in obesity: alteration of redox signaling. *Diabetes* 58(10):2189-2197.
13. Livak KJ & Schmittgen TD (2001) Analysis of relative gene expression data using real-time quantitative PCR and the 2(-Delta Delta C(T)) Method. *Methods* 25(4):402-408.